ELSEVIER

Journal of Power Sources 110 (2002) 152–162

JOURNAL OF POWER SOURCES

www.elsevier.com/locate/jpowsour

Rechargeable lithium/hybrid-electrolyte/pyrite battery

G. Ardel[a], D. Golodnitsky[a,*], K. Freedman[a], E. Peled[a], G.B. Appetecchi[b], P. Romagnoli[b], B. Scrosati[b]

[a]*School of Chemistry, Tel Aviv University, Tel Aviv 69978, Israel*
[b]*Department of Chemistry, University of La Sapienza, 00185 Rome, Italy*

Received 21 November 2001; received in revised form 21 March 2002; accepted 16 April 2002

Abstract

Different types of hybrid and gel polymer electrolytes (HPEs and GPEs) based on polymers and organic solvents combined with organic or inorganic gelation agents for Li/pyrite battery were studied. Ionic conductivity of 0.1–2.5 mS/cm at room temperature (RT) was achieved for HPE and 5 mS/cm for GPE. At 70 °C tetraglyme (TG)-based HPE had conductivities of 1–4 mS/cm, almost one order of magnitude higher than that of ''dry'' solid polymer electrolytes. An interfacial lithium/HPE resistance (R_{SEI}) of 6–10 Ω cm^2 was stable for about 3000 h. The specific capacity of the first discharge Li/pyrite cells with both HPEs and GPEs varied from 650 to 1000 mAh/g. The reversible specific capacity at 70 °C ranged from 250 to 600 mAh/g; the maximal capacity is similar to that of solid-electrolyte Li/FeS_2 batteries at 135 °C. After the initial capacity loss, stable cycling behavior with 0.1% per cycle degradation rate was observed.

Keywords: Lithium battery; Hybrid-electrode batteries; Pyrite battery

1. Introduction

With the rapid advances in mobile equipment and the growing interest in the development of electric and hybrid vehicles, new functions are being demanded for high energy–density rechargeable batteries. Systems with high energy–density on both a weight and a volume basis and high rate, attract considerable attention both of research and industry [1–3]. The balance between ecological and economical objectives is another but no less important factor. The abundance, low cost and high theoretical specific energy of the Li/FeS_2 couple (1273 Wh/kg based on 4e/FeS_2) make the natural mineral, pyrite, a promising cathode material for lithium batteries. The Li/composite polymer electrolyte (CPE)/pyrite battery with a 10 μm-thick cathode has a reversible capacity of 625 mAh/g (2.8e/FeS_2), which is about five times that of the Li/Li_xCoO_2 battery. Over 500, 100% DOD cycles with a capacity fading rate of less than 0.1% per cycle have been demonstrated in a small laboratory prototype Li/CPE/FeS_2 cell [4,5].

However, since solid polymer electrolytes have low ionic conductivity at ambient temperature, their application in lithium batteries is limited to elevated temperatures. In recent times, the need for polymer electrolyte batteries operating at near-ambient temperatures, has resulted in the development of gel (GPEs) and hybrid polymer electrolytes (HPEs), where macromolecular matrices, such as poly(acrylonitrile) (PAN), poly(vinyl chloride) (PVC) and poly(vinyl difluoride) (PVDF) immobilize common liquid electrolytes [6–14]. The range of GPE systems that have been characterized and developed for practical cells is extensive.

In the present work, we have directed our attention to the investigation of GPEs and HPEs for a ''green'' and cheap Li/pyrite battery.

2. Experimental

All materials were processed and cells were built inside argon filled VAC glove boxes. High purity, vacuum-dried components were used for polymer-film preparation. Solvents and plasticizers were dried for at least 48 h with molecular sieves. The procedure for the preparation of GPEs involved a sequence of several steps [15]: dissolution of a Li salt in the EC/DMC mixture; addition of PAN polymer component and its dispersion in the solution by stirring for several hours at room temperature (RT); transfer of the slurry to the preheated to 90 °C aluminum plate to promote fast PAN gelification and cooling of the gel to RT.

* Corresponding author. Tel.: +972-3-640-6879; fax: +972-3-640-9293.
E-mail address: golod@post.tau.ac.il (D. Golodnitsky).

0378-7753/02/$ – see front matter
PII: S0378-7753(02)00262-8

The chosen polymer for HPE is commercially available PVDF-2801 copolymer (Kynar). The PVDF powder was dissolved in high-purity cyclopentanone (Aldrich); fumed silica 130 (Degussa) or 15 nm-size alumina (Buehler) and propylene carbonate (PC, Merck), similar to the Bellcore process, were added and the mixture was stirred at room temperature for about 24 hours to get a homogeneous slurry. After complete dissolution, the slurry was cast on the Teflon support and spread with the use of the doctor-blade technique. To prevent surface irregularities, the film was then covered with a box pierced with holes that allowed a slow evaporation of the cyclopentanone.

After complete evaporation of the cyclopentanone, a 13 mm diameter disc was cut from the polymer membrane. It was soaked in LiI or LiImide-based electrolyte for 48 h. In order to ensure a complete exchange of the PC by electrolyte, at least three fresh portions of electrolyte were used for each soaking. LiI and LiImide-based electrolytes were stored in a glove box with Li chips. The porosity of membranes was estimated by comparing the mass of dry and soaked in different solvents films. Four types of liquid electrolytes based on solvents, such as: diglyme (DG), tetraglyme (TG), polyethylene glycol dimethyl ether (PEGDME, M_w 500) and a 1:1 (v/v) mixture of ethylene carbonate (EC) and dimethyl carbonate (DMC) were investigated. The compositions of GPEs and HPEs are presented in Table 1. In order to prevent polymerization of TG and PEGDME-based electrolytes the triethyl or tributyl amine inhibitor (1000 ppm) was added.

When the polymer disc was removed from the electrolyte solution, the surface was dried by light pressure on a laboratory wipe. The GPE or HPE discs were sandwiched between two lithium electrodes for conductivity and R_{SEI} measurements. All electrochemical tests were performed in hermetically sealed 1 cm^2 electrode area 2324 coin cells. For comparative studies, Celgard 2400 and Tefzel separators were used as matrices for hybrid polymer electrolytes.

Composite cathodes were prepared by the addition of 88.5% (w/w) pyrite to a mixture of 4.0% (w/w) PVDF (or Teflon) and 7.5% (w/w) SiO_2 in cyclopentanone. The blended paste was poured onto the graph-foil current collector and spread uniformly using the doctor-blade technique. Composite cathodes were dried in vacuum at 70 °C for 8 h. The area of the electrode was 1 cm^2.

The AC measurements were performed over a frequency range of 1 MHz to 5 Hz at an AC amplitude of 10 mV with a Solartron 1255-frequency response analyzer controlled by a 586 PC. The errors in the calculation of bulk and lithium interfacial resistance (R_{SEI}) were estimated to be about 10% at near ambient temperatures and 5% at 70 °C. Typically four identical cells were tested. Cell-cycling tests were carried out on a 16 bit Maccor 2000 battery tester at 50 μA/cm^2 over the voltage range of 2.3–1.1 V.

A JEOL SEM was used for the study of surface topology.

The samples for DSC measurements were prepared in a VAC glove box. Accurately weighted samples were hermetically sealed in high-pressure gold-coated stainless steel DSC pans. Such pans are completely inert to our system. We ran DSC test between metallic lithium and the pan. No reaction took place until 180 °C where a clear endotherm of Li melting is observed. The experimental value of the enthalpy of lithium fusion is equal to the theoretical one. DSC measurements were taken with TA Instruments module 2920 at a ramp rate of 10 °C/min.

Table 1
Composition and conductivity data of GPEs and HPEs

	Type of membrane	Composition of liquid electrolyte	σ ($\times 10^{-4}$ at RT, S/cm)	σ ($\times 10^{-4}$ at 70 °C, S/cm)
1	PVDF–SiO_2; 50% porosity	TG:1 M LiImide:10% (v/v) EC	9.0	33.0
2	PVDF–SiO_2; 75% porosity	TG:1 M LiImide:10% (v/v) EC	13.2	39.6
3	PVDF–Al_2O_3; 75% porosity	TG:1 M LiImide:10% (v/v) EC	13.6	42.9
4	Tefzel	TG:1 M LiImide:10% (v/v) EC	1.3	10.0
5	Celgard	DG:1.25 M LiImide:10% (v/v) EC	1.3	–
6	PVDF–SiO_2; 50% porosity	TG:1 M LiI:10% (v/v) EC	6.8	41.1
7	PVDF–SiO_2; 75% porosity	TG:1 M LiI:10% (v/v) EC	4.1	35.2
8	PVDF–Al_2O_3; 75% porosity	PEGDME:1 M LiImide:1% (v/v) EC	2.8	6.3
9	PVDF–Al_2O_3; 75% porosity	PEGDME:1 M LiI:1% (v/v) EC	1.7	4.4
10	PVDF–Al_2O_3; 75% porosity	PEGDME:1.5 M LiI:1% (v/v) EC	1.8	7.0
11	PVDF–Al_2O_3; 75% porosity	PEGDME:2 M LiI:1% (v/v) EC	2.6	7.7
12	Celgard	PEGDME:1 M LiI:1% (v/v) EC	0.5	1.0
13	Celgard	PEGDME:1.5 M LiI:1% (v/v) EC	0.6	–
14	Celgard	PEGDME:2 M LiI:1% (v/v) EC	0.7	–
15	PVDF–SiO_2; 50% porosity	DMC:EC (1:1):1 M LiImide	18.8	–
16	PVDF–SiO_2; 50% porosity	DMC:EC (9:1):1 M LiImide	20.0	–
17	PAN	DMC:EC (1:1):1 M $LiPF_6$	48.0	–

3. Results and discussion

3.1. SEM and DSC characterization

The membranes for HPEs were transparent or slightly translucent with a smooth surface. As can be seen from the SEM micrographs (Fig. 1) even at high magnification (20,000×) the topography of PVDF–SiO_2 membranes is very homogeneous with no cracks. The surface presents a multitude of compacted PVDF grains (possibly spherulites). In the membrane with 75% porosity the grains are less compacted and connected by polymer filaments liberating more space for pores. In fact, a picture of the bulk cross-section morphology of this membrane (Fig. 1c) exhibits a completely porous structure evocative of a sponge. The membrane with 50% porosity shows more compact bulk morphology (Fig. 1d). The alumina-containing membrane is built from several micron-size closely packed aggregates (Fig. 2). In the cross-section view of the membrane, cavities can be distinguished (Fig. 2c). Tefzel has a porous rubber-like structure (Fig. 2d–f)

The sample with alumina (75% porosity) has good mechanical strength (10 MPa) and extremely high ductility. The less porous SiO_2-based membrane has better mechanical properties (14 Mpa), but the elongation of this membrane did not exceed 15%. Both membranes were easily worked. The samples of all the membranes were found to enable the high electrolyte uptake (up to 130–150%). DMC-EC and PEG based HPEs are free-standing easy worked films with similar mechanical properties.

Figs. 3 and 4 represent DSC thermograms of the TG-based liquid and HPEs with LiI and LiImide salts. As the temperature is lowered the LiI–TG electrolytes and the related HPE undergo crystallization in the vicinity of −40 °C (Fig. 3), while LiImide–TG do not (Fig. 4), the latter being a glass-forming liquid. The strong peak at −40 °C (Fig. 3) is attributed to the melting of LiI–TG complex. It is supposed that lithium can form several complexes with TG differing by coordination number. Two close endothermic peaks at about RT may be associated with melting of Li–EC complex and partial decomposition of Li–TG complex, induced by polymer membrane. A weak transition observed at 60 °C is possibly related to the melting of some polymerized (CH_2–CH_2–O) chains with $n > 4$. As is clear from the figures, DSC thermograms of both liquid and the corresponding HPEs are essentially identical. However, the ratio between enthalpy values of the endothermic events and their kinetics, differ substantially for liquid and HPEs. For instance, in the LiI–TG liquid electrolyte (Fig. 3, curve 1) the enthalpy of the peak −40 °C (53.2 J/g) is more than one order of magnitude larger than the sum of enthalpies of the other two peaks (1.6 J/g), and more than two

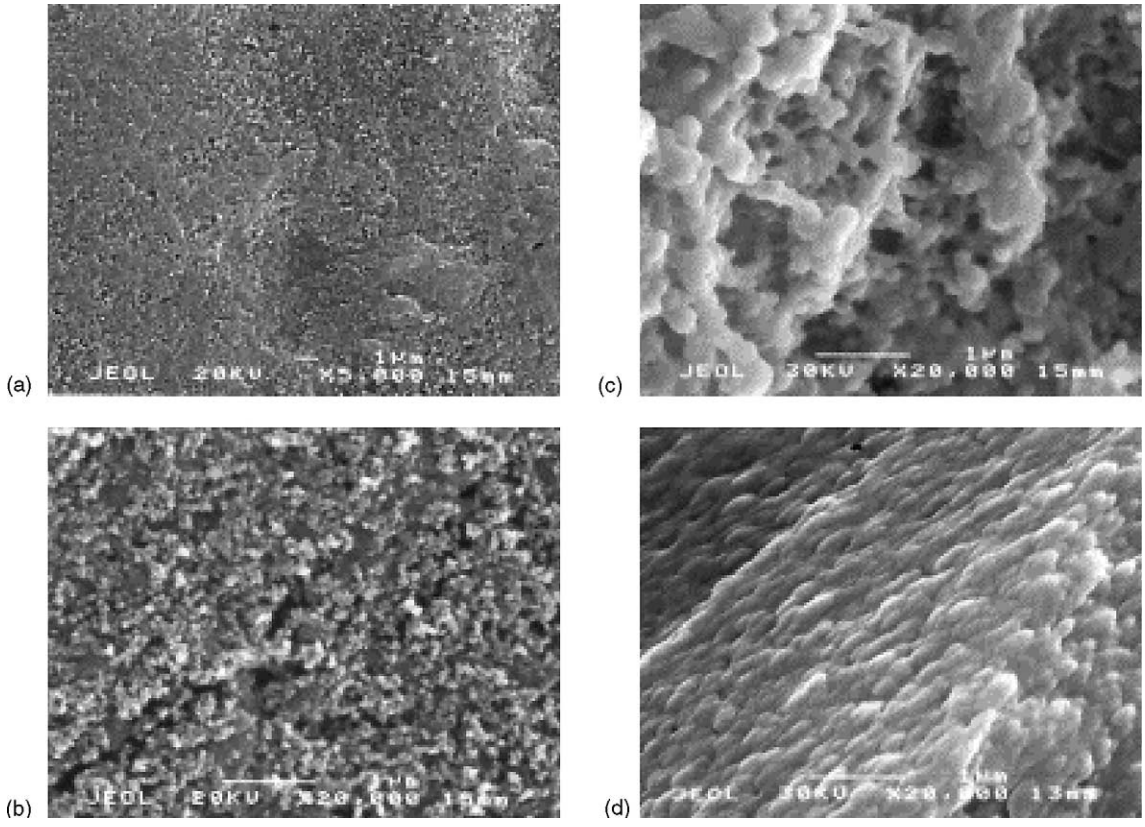

Fig. 1. SEM micrographs of PVDF–SiO_2 membranes: (a) and (b) surface morphology; (c) and (d) cross section view of 75 and 50% (v/v) porous films, respectively.

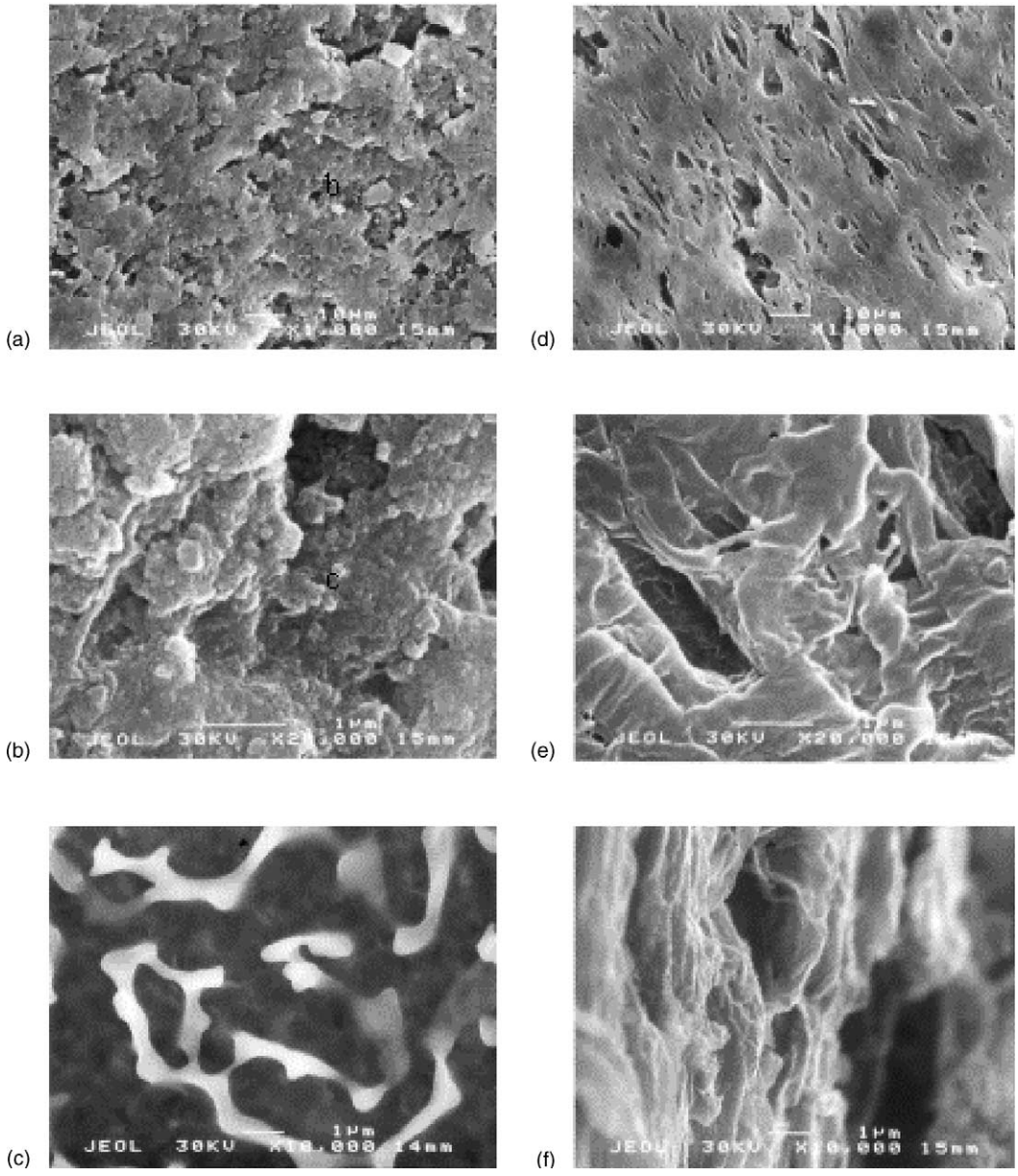

Fig. 2. SEM micrographs of PVDF–Al_2O_3 (a–c) and Tefzel (d–f) membranes; (c) and (d) cross section view.

orders of magnitude larger than that of the endotherm peak (0.3 J/g), at 60 °C. In the corresponding HPEs there is the overlapping of the two endotherms peaks. A clear shift of the peak toward lower temperature is observed, the difference between enthalpies of the observed phase transitions decreases and they become energy-comparable. Similar phenomena are observed for the LiImide–TG HPEs (Fig. 4). Here also, the gap between enthalpies of the endothermic transitions is significantly lower in the HPE. In addition, the endotherm peak in the HPE shifts toward lower temperature by 12 °C as compared to that in the liquid electrolyte. Since crystallization and melting of the liquid would be sensitive to the environment, this behavior, as expected, may indicate some kind of interaction between the polymer matrix and the electrolyte.

3.2. Conductivity measurements

The conductivity data of the GPEs and HPEs under investigation are collected in Table 1. The highest values of ionic conductivity at RT (2–4 mS/cm) were measured for EC:DMC HPEs and PAN-based GPE.

PVDF is an ‘‘electrolyte starved membrane’’ for which the magnitude of the conductivity is dependent upon polymer porosity. As can be seen from the data presented in Table 1, as the volume fraction of PVDF in starting mixture increases (porosity decreases) the conductivity becomes lower both at RT and at 70 °C. Alumina- and silica-containing HPEs show similar conductivity values. However, the conductivity of Tefzel- and Celgard-based HPEs with LiImide–TG liquid electrolyte is about one order of magnitude

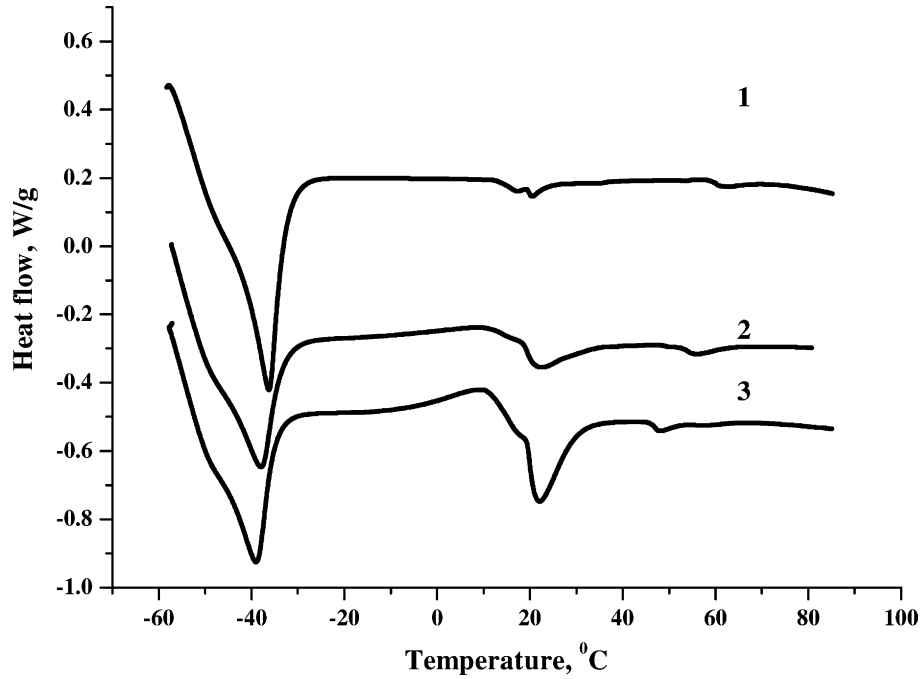

Fig. 3. DSC thermograms of liquid 1 M LiI, TG, EC (1% (v/v)) electrolyte (1) and corresponding HPE (2) and (3) with 50 and 75% porous PVDF–silica membranes.

lower at RT and 4 times lower at 70 °C. This is mostly due to the poor wetting properties of these membranes. LiImide–TG and LiImide–PEGDME liquid electrolytes trapped in PVDF–silica matrix are generally more conductive than those containing lithium iodide salt. This is in agreement with the formation of less crystalline complexes as found by DSC.

At 70 °C the conductivity of hybrid TG-based electrolytes with both LiI and LiImide salts is almost one order of magnitude higher than that of "dry" solid PEO-based polymer electrolytes.

PEGDME-based HPEs showed conductivity values lower by a factor of five–seven as compared to those of

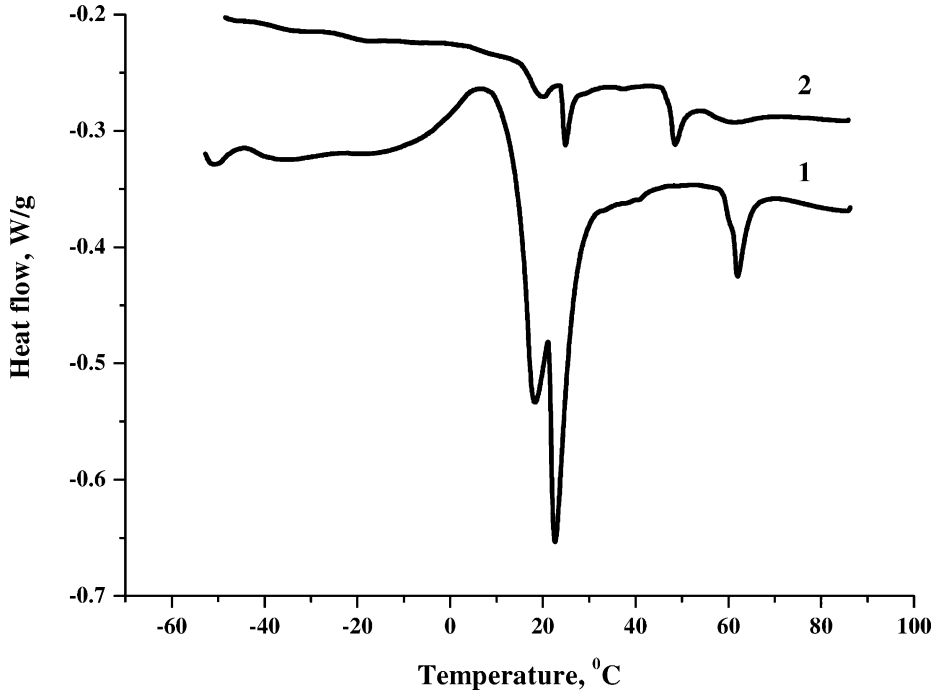

Fig. 4. DSC thermograms of liquid 1 M LiImide, TG, EC (1% (v/v)) electrolyte (1) and corresponding HPE (2). Membrane composition (75% porosity): 15% (v/v) PVDF and 10% (v/v) fumed silica.

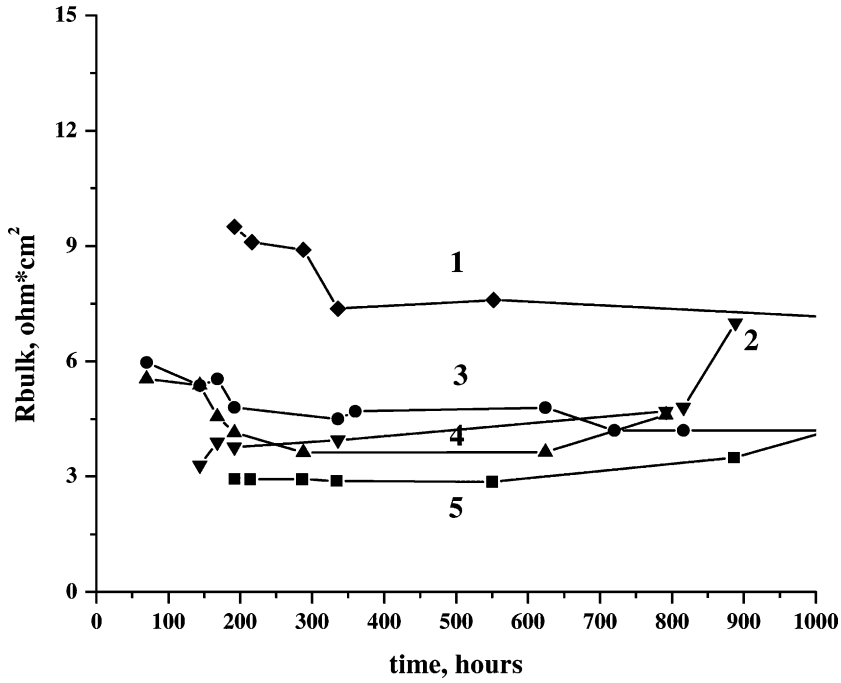

Fig. 5. Effect of time of storage on the bulk resistance of HPEs at 70 °C: (1) LiI-based electrolyte with 75% porous PVDF–SiO_2 membrane; (2) LiImide-based electrolyte with 75% porous PVDF–Al_2O_3 membrane; (3) LiImide-based electrolyte with 50% porous PVDF–SiO_2 membrane; (4) LiI-based electrolyte with 50% porous PVDF–SiO_2 membrane; (5) LiImide-based electrolyte with 75% porous PVDF–SiO_2 membrane. Liquid electrolyte composition: TG, 1 M LiImide or LiI, 10% (v/v) EC, 1000 ppm tetrabutyl amine.

TG-based HPEs. This may be caused by the higher viscosity of the former solvent and hampered segmental motion of the long-chain PEGDME inside the pores of membrane.

Increasing the lithium iodide concentration from 1 to 2 M results in an increase in RT conductivity of the PVDF–SiO_2 HPEs by a factor of 1.5. The effect of salt concentration on the ionic conductivity is more pronounced at elevated

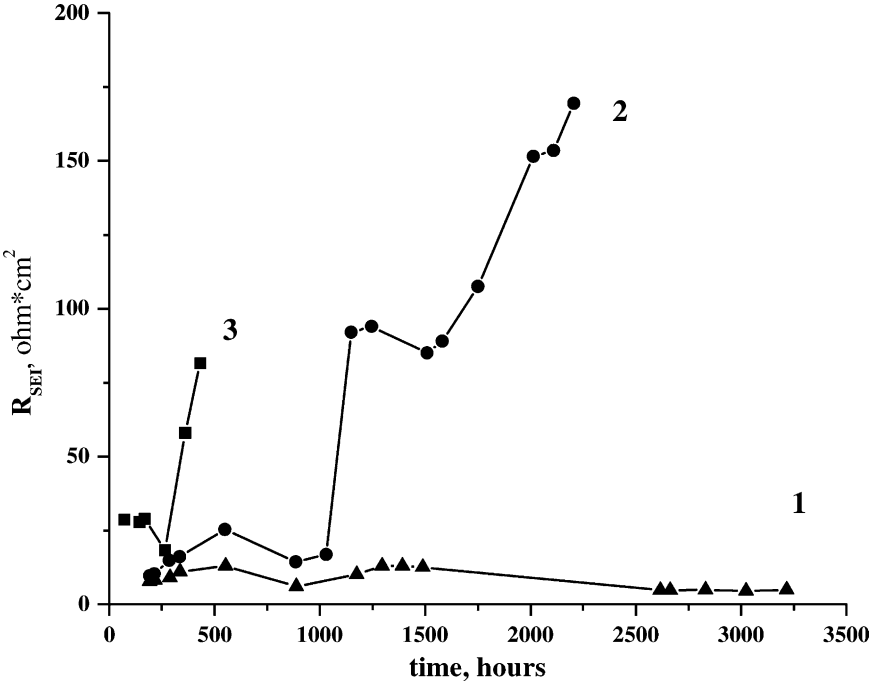

Fig. 6. Effect of time of storage on the SEI in Li/HPEs/Li cells at 70 °C. HPE composition: (1) 1 M LiI, TG, 10% (v/v) EC, 75% porous PVDF–SiO_2 membrane; (2) 1 M LiImide, TG, 10% (v/v) EC, 75% porous PVDF–SiO_2 membrane; (3) 1 M LiImide, TG, 10% (v/v) EC, Tefzel membrane. All HPEs contain 1000 ppm tetrabutyl amine.

temperatures. It seems likely that in the HPEs the PVDF–polymer matrix does not behave like a quasi-inert cage for the solution, although the specific nature and the level of the ion–polymer interaction remain unknown yet.

A property of polymer electrolytes of importance equal to that of high absolute value of ionic conductivity is the stability of bulk resistance (R_b). The effect of storage time on the change of the R_b at 70 °C (Fig. 5) shows that the bulk resistance of the HPEs with both LiI and LiImide–TG electrolytes remains almost constant (3–10 Ω cm^2) for more than 1000 h. This indicates good physical integrity of the membranes and liquid electrolytes, which do not experience evaporation and extensive polymerization of solvents.

3.3. Li/HPE and Li/GPE interfacial properties

Compatability of the electrolyte with anode and cathode materials and the stability of the anode/electrolyte and cathode/electrolyte interfaces are essential for the success of an advanced battery. The impedance of the SEI (R_{SEI}) formed on lithium largely determines the total impedance of the battery, thus affecting cell behavior in terms of cycleability, rate and safety [16,17]. The evolution of the SEI impedance at the Li/electrolyte interface as a function of the storage time is shown in Fig. 6. LiI–TG-based HPEs form SEIs that are highly stable for more than 3000 h. The threefold increase in the R_{SEI} of LiImide HPEs after 300 h of storage and about an order of magnitude increase after 2000 h, provides evidence of the thickening with time of the passivation layer on lithium. The effect of salt on the stability of the SEI was similar in the PVDF–SiO_2 and PVDF–Al_2O_3 HPEs of different porosity. Low and almost constant resistance of the SEI in lithium iodide-containing electrolytes may be associated with high thermodynamic stability of the iodide anion towards metallic lithium.

In HPEs with Tefzel membranes even the initial R_{SEI} value was twice that in HPEs with PVDF membrane, and the R_{SEI} increased sharply (up to 80 Ω cm^2) after 300 h of storage (Fig. 6). These data support previous observations that nano-size ceramic fillers incorporated in polymer membrane decrease and stabilize interfacial resistance in hybrid as well as in composite solid polymer electrolytes [18,19]; this is due to their ability to adsorb impurities and traces of water. In addition, inorganic fillers may prevent free diffusion of the liquid electrolyte components to the lithium surface and, as a result, inhibit the growth of the SEI. It is worth noting that the resistance of the lithium passive film in alumina-containing HPEs is twice that in the silica-based HPEs. The same R_{SEI} difference was detected between Al_2O_3- and SiO_2 high-porous and less porous HPEs. At RT, the initial R_{SEI} in the LiI–TG- and LiI–PEGDME-based HPEs was about 200 Ω cm^2, while in LiImide it was 280 Ω cm^2. After 200 h of storage the R_{SEI} increased by about 10% in the former electrolyte and by about 25% in the latter.

The initial interfacial resistance of EC:DMC–PAN-based GPEs at RT was about the same order of magnitude as in TG-, PEGDME- and EC:DMC-based HPEs. The R_{SEI} stability, however, was much lower than that of the HPEs and the R_{SEI} increased up to 1.5 kΩ after 900 h of storage [9]. Thus, doubts are raised as to the inert nature of the PAN matrix with respect to Li passivation. The reactivity of PAN may stem from impurities in the commercial product and reactivity of the –CN group possibly leading to the formation of LiCN. Dissolution of LiCN could be followed by the breaking of and thickening the SEI. Contrary to EC:DMC

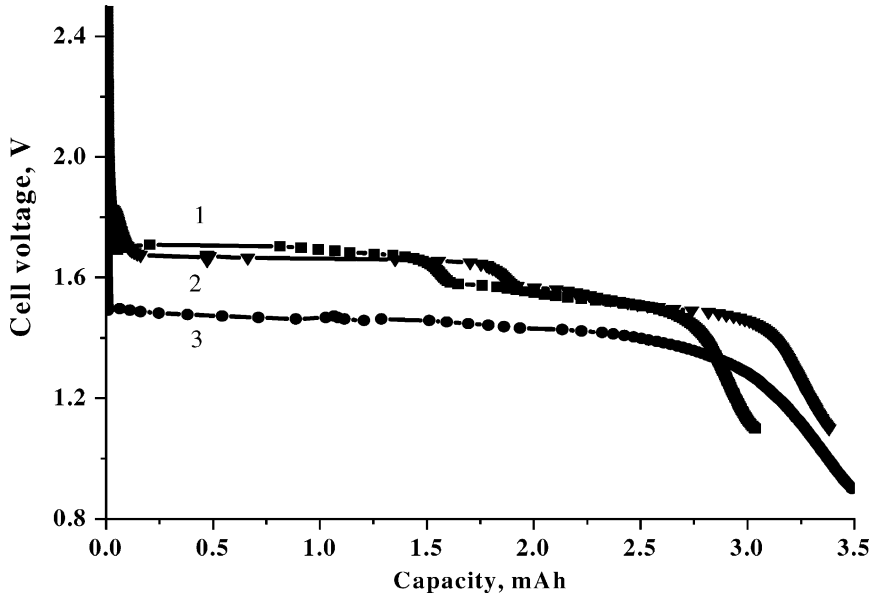

Fig. 7. First discharge of the Li/HPE/pyrite cells at RT (3) and at 70 °C (1 and 2). (1) 1 M LiImide, PEGDME, EC (1% (v/v)), Celgard; (2) 1 M LiI, PEGDME, EC (1% (v/v)), 75% porous PVDF–Al_2O_3 membrane; (3) 1 M LiImide, DMC:EC (1:1), 75% porous PVDF–SiO_2 membrane $I_d = 0.05$ mA/cm^2.

solvents, lithium oxide, carbonate, fluoride compounds and alkoxides, which are the basic compounds found in the anode SEI, are highly insoluble in TG and PEGDME solvents similar to solid PEO [17]. This property, as expected, increases the stability of the lithium passivation layer by producing a thinner and more compact film.

3.4. Li/HPE and GPE/pyrite batteries

Li/pyrite batteries with GPEs and HPEs were tested in this work. The first discharge of lithium/HPE/FeS_2 cells (Fig. 7, curve 3) at RT showed a single plateau at 1.5 V. The specific capacity of the first discharge of the cells at RT varied from 650 to 1000 mAh/g depending on the electrolyte composition. At 70 °C two well defined plateaus at 1.7 and 1.5 V were observed on first discharge (Fig. 7, curves 1 and 2). This indicates that, as with non-aqueous and polymer electrolytes, the reduction of FeS_2 proceeds as a multi-stage process, first to FeS or Li_2FeS_2 and finally to metallic iron [20–24]. The single plateau seen for the RT cells suggests that the two steps in the pyrite reduction proceed simultaneously.

Addition of EC to the LiImide–PEGDME HPE was followed by an increase of about 10% in the first discharge capacity. The first-discharge utilization of cathode-active material did not change on substitution of LiImide by LiI.

Contrary to what might be expected from the non-reversible behavior of pyrite in non-aqueous electrolytes, such as: dioxolane, tetrahydrofuran, propylene carbonate (PC) and 1:2 dimethoxyethane in non-aqueous solvents [20–23] we have found that Li/hybrid or GPE/pyrite cells are rechargeable even at RT (Fig. 8). Reversible specific capacity for the second cycle was about 250 to 600 mAh/g; the upper value of capacity is similar to that of solid electrolyte batteries at 135 °C.

All the subsequent discharge curves differ from the first one indicating a change in the initial mechanism of pyrite reduction. Analysis of the dQ/dV curves (Fig. 9) showed that charge–discharge processes in the Li/FeS_2 battery with

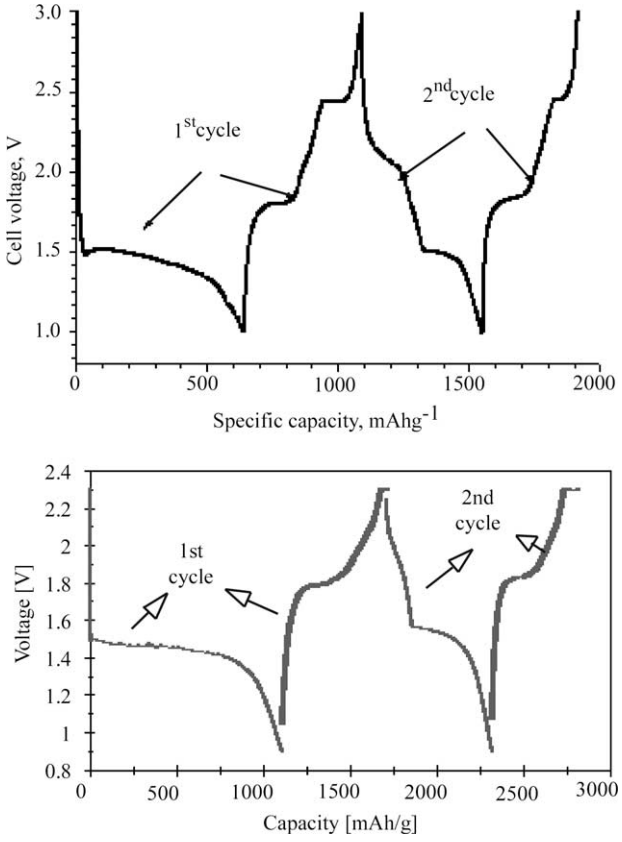

Fig. 8. Voltage profiles of discharge–charge process of Li/HPE or GPE/FeS_2 battery at RT, $I_d = 0.05$ mA/cm^2, $I_{ch} = 0.05$ mA/cm^2. (1) HPE, 1 M LiImide, DMC:EC (1:1), 75% porous PVDF–SiO_2 membrane; (2) GPE, $LiClO_4$ $EC_{56.5}$:$DMC_{23}PAN_{16}$.

HPEs at RT and at 70 °C are similar. Substitution of the LiImide by LiI, PEG by TG and the PVDF-based membrane by Celgard in HPEs did not substantially affect the main reversible phases formed on the second charge–discharge cycle of pyrite. Two types of pyrite-based cathodes with PVDF and Teflon binders were tested in LiImide–PEG

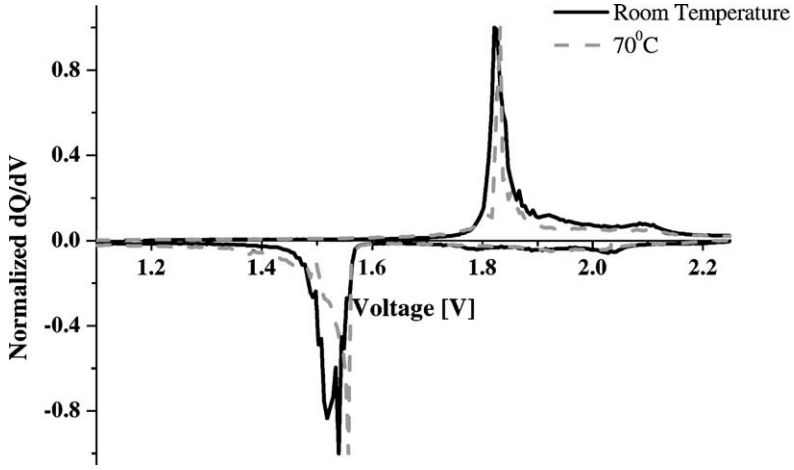

Fig. 9. The dQ/dV curves of Li/HPE/FeS_2 cell at RT and 70 °C (second cycle). Electrolytes composition: 1 M LiImide, $PEGDME^{500}$, EC (1% (v/v)), at 70 °C 1 M LiImide, DMC:EC (1:1), at RT 75% porous PVDF–SiO_2 membrane, $I_d = 0.05$ mA/cm^2, $I_{ch} = 0.05$ mA/cm^2.

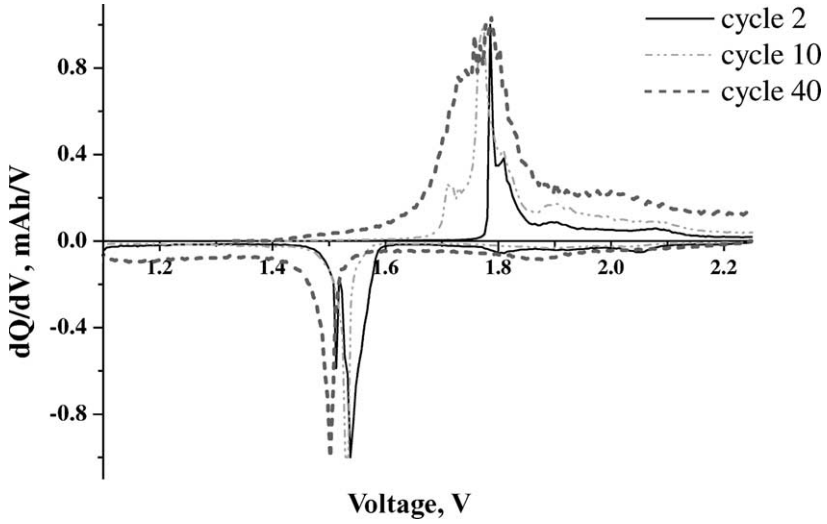

Fig. 10. The dQ/dV curves of Li/HPE/FeS_2 cell (normalized capacity) at 70 °C. Electrolyte composition: 1 M LiImide, $PEGDME^{500}$, EC (1% (v/v)), 60% porous PVDF–SiO_2 membrane, Teflon-bonded cathode $I_d = 0.05$ mA/cm^2, $I_{ch} = 0.05$ mA/cm^2.

HPEs. As can be seen from Fig. 10, long-term cycling of the Li/HPE/pyrite cell with Teflon-based cathode results in broadening and overlapping of the charging dQ/dV peaks, and about a 30 mV increase in the discharge overpotential.

On the basis of the experimental data, the charge process, which is reversible from the second cycle on, can be schematically described by reactions (1) and (2), which were also ascribed to the Li/solid CPE/pyrite cell [24–27]:

$$Fe + 2Li_2S - 2e \rightarrow Li_2FeS_2 + 2Li^+ \quad (1)$$

$$Li_2FeS_2 - X\,Li^+ - Xe \rightarrow Li_{2-x}FeS_2 \quad (0.5 < X < 0.8) \quad (2)$$

Broadening of the charging dQ/dV peaks and increase in the relative capacity of the shoulder at 1.7 V, which has no corresponding cathodic peak, (Fig. 10) may be associated with slow mass transport of iron(II) cations through the Li_2FeS_2 phase [27]. On the other hand, the formation of an FeS intermediate followed by a slow reaction (3) cannot be ruled out.

$$FeS + Li_2S \rightarrow Li_2FeS_2 \quad (3)$$

Over 20 cycles with degradation rate of 2.1% per cycle were obtained for the RT Li/TG-based HPE/FeS_2 cells (Fig. 11). The capacity loss was attributed to the partial loss of electrical contact in between cathode-active material particles and between the graph-foil current collector. This is due to the partial dissolution in the TG-solvent at RT of the PVDF binder used in the composite cathode. Similar phenomenon was found in PEG at 70 °C.

In Li/EC:DMC PAN/Teflon-bonded composite-pyrite cathode cells, operating at RT, the capacity loss was 2.6% per cycle. The Faradaic efficiency was about 95%. It seems likely that in this case high and unstable interfacial resistance may cause the high degradation rate observed. This makes passive-layer formation at the Li/PE interface the dominating factor in the recharging ability of cells. For the Li/HPE/pyrite cells operating at 70 °C over 130 cycles with capacity loss of 0.1% per cycle and estimated reversible capacity of 300–400 mAh/g were achieved (Fig. 12).

3.5. Safety tests

Although the replacement of liquid electrolyte by GPEs and HPEs should improve the safety of lithium batteries some concerns remain. Cells deliberately heated to high temperatures can eventually undergo thermal runaway reactions and become a safety hazard. DSC tests were used in the study of the reactivity of battery materials. In Fig. 13 are shown the DSC thermograms of a composite cathode, LiI–TG–PVDF–SiO_2-HPE, and the HPE with metallic lithium. As can be seen from DSC (curves 1 and 2), no thermal events occur until 200 °C. With solvents in contact with lithium (curve 3) the enthalpy of this exotherm increases, as a result of a possible interaction of the molten lithium (see endothermic peak at 180 °C) and vapors. It should be mentioned, however, that until 275 °C no thermal runaway is observed, indicating stability and safety of the system under operating conditions.

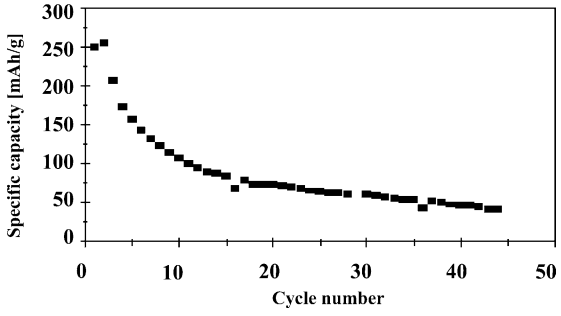

Fig. 11. Cycle life of Li/HPE/FeS_2 cell at RT. Electrolyte composition: 1 M LiImide, DMC:EC (1:1), 75% porous PVDF–SiO_2 membrane, PVDF-bonded cathode, $I_d = 0.05$ mA/cm^2, $I_{ch} = 0.05$ mA/cm^2.

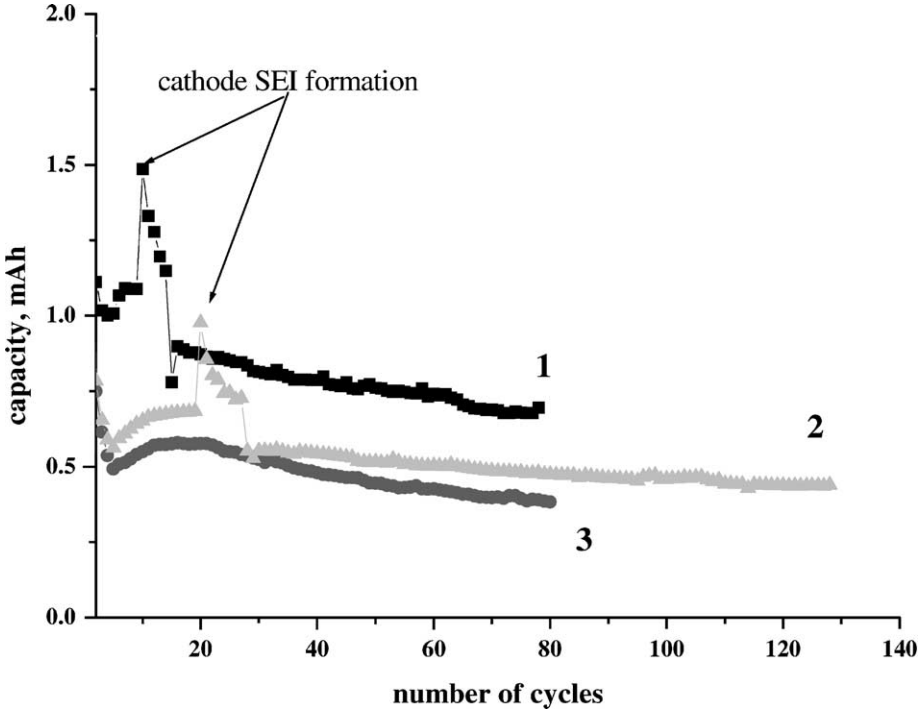

Fig. 12. Cycle life of Li/HPE/FeS_2 cell at 70 °C. Electrolyte composition: 1 M LiImide, $PEGDME^{500}$, EC (1% (v/v)), 60% porous PVDF–SiO_2 membrane, Teflon-bonded composite cathode, $I_d = 0.05$ mA/cm^2, $I_{ch} = 0.05$ mA/cm^2.

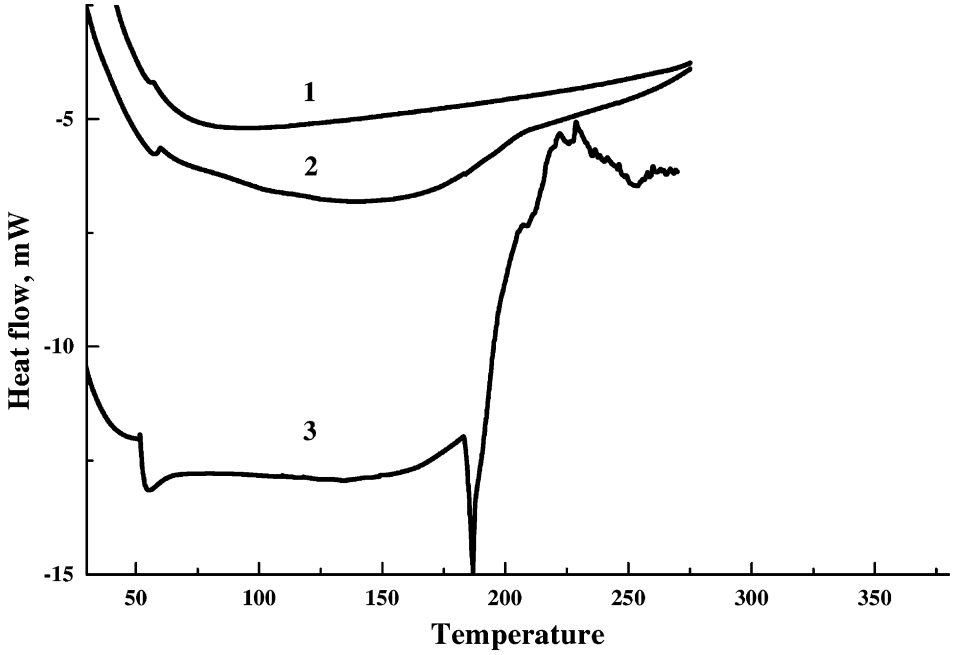

Fig. 13. DSC runs of: (1) composite pyrite-based cathode; (2) HPE (1 M LiI, TG, EC (1% (v/v)) 75% porous PVDF–SiO_2 membrane; (3) HPE in contact with metallic lithium.

4. Summary

Different types of HPEs and GPEs based on polymers and organic solvents combined with organic or inorganic gelation agents for the Li/pyrite battery were studied. The morphology of membranes used in hybrid polymer electrolytes depends on porosity and inorganic filler. DSC tests indicate possible interaction of the polymer host and liquid electrolyte.

Ionic conductivities of 1×10^{-4} to 4×10^{-3} S/cm at RT and at 70 °C were achieved in GPEs and HPEs, almost one order of magnitude higher than that of solid polymer

electrolytes. In Li/HPE/FeS_2 battery at 70 °C the R_{SEI} of 6–10 $\Omega\,cm^2$ was stable for more than 3000 h.

The analysis of dQ/dV curves showed that charge–discharge process in the Li/gel or HPE/FeS_2 battery is similar to that of the Li/LiI-PEO_{20}12%Al_2O_3/pyrite battery. Reversible specific capacity for the second cycle was about 250 to 600 mAh/g; the maximal capacity similar to that of solid electrolyte batteries at 135 °C. Over 20 cycles with a degradation rate of 2.1–2.6% per cycle were obtained for the RT cells and over 130 cycles with a capacity loss of 0.1% per cycle for the cells at 70 °C. The stability and safety of the Li/HPE/FeS_2 battery up to 275 °C was demonstrated.

Acknowledgements

The TAU group would like to thank the Israel Ministry of Energy for financial support. The Italian laboratory is grateful to ENEA for financial support under contract 9981.

References

[1] D. Linden, Handbook of Batteries, McGray-Hill Book Company, 1995, pp. 14.1–14.90.
[2] L. Dominey, Lithium Batteries: New Materials, Developments and Perspectives, Elsevier, Amsterdam, 1994, p. 137.
[3] J.O. Besenhard (Ed.), Handbook of Battery Materials, Wiley, New York, 1999.
[4] E. Peled, D. Golodnitsky, G. Ardel, J. Lang, Y. Lavi, J. Power Sources 54 (1995) 495.
[5] D. Golodnitsky, E. Peled, Electrochim. Acta 1/2 (45) (1999) 335.
[6] K.M. Abraham, in: B. Scrosati (Ed.), Applications of Conductive Polymers, Chapman & Hall, London, 1993, p. 182.
[7] B. Scrosati, C.A. Vincent, MRS Bull. 3 (2000) 31.
[8] M. Kono, E. Hayashi, M. Nishiura, M. Watanabe, J. Electrochem. Soc. 147 (7) (2000) 2517.
[9] H.-J. Ryoo, H.-T. Kim, Y.-G. Lee, J.-K. Park, S.-I. Moon, J. Solid State Electrochem. 3 (1998) 1–6.
[10] C.S. Kim, S.M. Oh, Electrochim. Acta 46 (2001) 1323.
[11] G.B. Appetecchi, F. Croce, B. Scrosati, Electrochim. Acta 40 (1994) 991.
[12] J.-M. Tarascon, A.S. Gozdz, C. Schmutz, F. Shokoohi, P.C. Warren, Solid State Ionics 86–88 (1996) 49.
[13] I.I. Olsen, R. Koksbang, J. Electrochem. Soc. 143 (1996) 570.
[14] O. Bohnke, G. Frand, Solid State Ionics 66 (1993) 97.
[15] G.B. Appetecchi, F. Croce, P. Romagnoli, B. Scrosati, U. Heider, R. Oesten, Electrochem. Commun. 1 (1999) 83–88.
[16] E. Peled, J. Electrochem. Soc. 126 (1979) 2047.
[17] E. Peled, D. Golodnitsky, J. Penciner, in: J.O. Besenhard (Ed.), Handbook of Battery Materials, Wiley, New York, 1999, p. 419.
[18] E. Peled, D. Golodnitsky, G. Ardel, V. Eshkenazy, Electrochim. Acta 40 (1995) 2197.
[19] G.B. Appetecchi, F. Croce, L. Persi, F. Ronci, B. Scrosati, Electrochim. Acta 45 (2000) 1481–1490.
[20] G.L. Henriksen, Lithium/iron sulfide batteries, in: Handbook of Batteries, 1995, pp. 39.1–39.17.
[21] M.B. Clark, Lithium–iron disulfide cells, in: J.P. Gabano (Ed.), Lithium Batteries, Academic Press, New York, 1983, pp. 115–135.
[22] S.K. Preto, Z. Tomczuk, S. von Winbusch, M.F. Roche, J. Electrochem. Soc. 130 (1983) 264.
[23] R. Fong, J.R. Dahn, C.H.W. Jones, J. Electrochem. Soc. 136 (1989) 11.
[24] D.A. Scherson, The Electrochemical Society Interface, Fall, 1996, p. 34.
[25] D. Golodnitsky, E. Peled, Electrochim. Acta 1/2 (45) (1999) 335–351.
[26] E. Strauss, D. Golodnitsky, E. Peled, Electrochim. Acta 45 (8/9) (2000) 1519–1525.
[27] E. Strauss, D. Golodnitsky, E. Peled, J. Solid State Electrochem., in press.